BNL-97087-2012-CP

Duplex Oxide Formation during Transient Oxidation of Cu-5%Ni(001) Investigated by In situ UHV-TEM and XPS

Yihong Kang[a], Langli Luo[b], Xiao Tong[c], David Starr[c], Guangwen Zhou[b], Judith C. Yang[d]

[a]Department of Mechanical Engineering and Materials Science, University of Pittsburgh, Pittsburgh, PA, USA
[b]Department of Mechanical Engineering & Multidisciplinary Program in Materials Science and Engineering, State University of New York, Binghamton, NY, USA
[c]Center for Functional Nanomaterials, Brookhaven national laboratory, Upton, NY, USA
[d]Department of Chemical and Petroleum Engineering, University of Pittsburgh, Pittsburgh, PA, USA

Presented at the 8th International Symposium on High Temperature Corrosion and Protection of Materials (HTCPM 2012)

Les Embiez, France
May 20 – 25, 2012

March 2012

Center for Functional Nanomaterials

Brookhaven National Laboratory

U.S. Department of Energy
DOE - OFFICE OF SCIENCE

DISCLAIMER

Duplex Oxide Formation during Transient Oxidation of Cu-5%Ni(001) Investigated by *In situ* UHV-TEM and XPS

Yihong Kang[a], Langli Luo[b], Xiao Tong[c], David Starr[c], Guangwen Zhou[b],

Judith C. Yang[d]

[a]*Department of mechanical engineering and materials science, University of Pittsburgh, Pittsburgh, Pa 15261, USA*

[b]*Department of mechanical engineering & multidisciplinary program in materials science and engineering, State University of New York, Binghamton, NY 13902, USA*

[c]*Center for functional nanomaterials, Brookhaven national laboratory, Upton, NY 11973*

[d]*Department of chemical and petroleum engineering, University of Pittsburgh, Pittsburgh, PA 15261, USA*

yik3@pitt.edu, *langley821@gmail.com*, *xtong@bnl.gov*, *dstarr@bnl.gov*, *gzhou@binghamton.edu*, *judyyang@pitt.edu*

Abstract. The transient oxidation stage of a model metal alloy thin film was characterized with *in situ* ultra-high vacuum (UHV) transmission electron microscopy (TEM), X-ray photoelectron spectroscopy (XPS) and analytic high-resolution TEM. We observed the formations of nanosized NiO and Cu_2O islands when Cu-5a5%Ni(100) was exposed to oxygen partial pressure, $pO_2=1\times10^{-4}\ Torr$ and various temperatures *in situ*. At 350 ℃ epitaxial Cu_2O islands formed initially and then NiO islands appeared on the surface of the Cu_2O island, whereas at 750 ℃ NiO appeared first. XPS and TEM was used to reveal a sequential formation of NiO and then Cu_2O islands at 550 ℃. The temperature-dependant oxide selection may be due to an increase of the diffusivity of Ni in Cu with increasing temperature.

Keywords: Cu-Ni, oxidation, in situ, TEM

INTRODUCTION

Wagner theory predicts the oxide scale morphology based on the relative amounts of the oxidizing components that well describes the oxidation behavior of metallic alloys [1]. However, these descriptions of the oxide scale morphology are applicable for the later stages of oxide scale growth and are qualitative. These macroscopic depictions miss how initial surface conditions and early stages of oxidation lead to the final oxide scale morphology, though it is well-known that surface conditions and secondary elements dramatically impact the oxide structure. The general sequence of metal oxidation is oxygen chemisorption, nucleation and growth of oxide, and bulk oxide growth. [2-12].

Visualizing the oxidation process at the nanometer scale with *in situ* experiments under ultra high vacuum conditions provides essential insights into the complex kinetics and energetics of nano-oxide formation. *In situ* transmission electron microscopy (TEM) allows us to study the nucleation and growth processes of oxide, provides a unique view of dynamic reactions as they occur at the nanometer regime and below, and bridges the gap between surface science studies and bulk oxidation or corrosion investigations. The dynamic information obtained from these *in situ* experiments enables us to understand and therefore manipulate the initial surface reactions that control the macroscopic scale morphologies.

Here, we report our initial oxidation results of a model metal alloys system, Cu-5%Ni, as an extension of our prior work of Cu and Cu-Au *in situ* oxidation[13-22]. Our extensive research on Cu oxidation have demonstrated that oxidation involves nucleation and growth, surface diffusion and solid state reactions, and bears a striking resemblance to heteroepitaxy [15, 17, 18]. Early-stage oxidation of both Cu and Ni has been extensively studied,[23-29] but little is known regarding the oxidation of Cu-Ni alloy. The Cu-Ni alloys will show more complex behavior, where the two components are 100% solid-soluble down to ~300 ℃ but Cu_2O and NiO show very limited miscibility. Nickel oxide, which has the cubic NaCl crystal structure with a =4.195 nm, has a more negative standard free energy of formation than Cu_2O, which is simple cubic with a =4.269 nm, and is expected to form more readily. In this case, depending on pO_2, either one or both components of the alloy will oxidize, thus enabling systematic determination of the effects of compositional and phase development during oxidation. Such insights into selective oxidation behavior of alloys are of significant importance since multiple elements are added to materials to provide optimal performance in an oxidizing environment.

EXPERIMENTAL PROCEDURES

The microscope used in this work was a modified JEOL 200CX. A leak valve attached to the column of the microscope permits the introduction of gases directly into the microscope. In order to minimize the contamination, a UHV chamber was attached to the middle of the column, where the base pressure was less than 10^{-8} Torr without the use of the cryoshroud. The cryoshroud inside the microscope column can reduce the base pressure to approximately 10^{-9} Torr when filled with liquid helium. For more details about the experimental apparatus, see McDonald et al. [30]

Single crystal 80 nm thick Cu-5at%Ni(100) thin films were deposited onto NaCl (100) substrates using a Pascal dual-gun UHV e-beam evaporator by simultaneous evaporation of 99.999% pure Cu and Ni at 380℃. The films were removed from the substrate by dissolving the NaCl in de-ionized water, washed and then mounted on a top-entry TEM holder which can be resistively heated up to 1000 ℃ *in situ*. Gas can be admitted into the column of the microscope through the leak valve at a pressure of 5×10^{-5} to 760 Torr. The Cu-Ni film formed a native oxide on the surface due to air exposure. Before

oxidation *in situ*, the native oxide of Cu-Ni film was reduced inside the TEM by annealing the Cu-Ni films at 750°C within an Ar plus 2%H_2 gas mixture at a pressure of 5×10^{-4} Torr. To oxidize the Cu film, scientific grade oxygen gas (99.999% purity) was introduced into the TEM chamber at a partial pressure of $5x10^{-4}$Torr and temperatures between 500 and 700 ℃. A Gatan SC1000 Orius™ CCD camera was used to capture the oxidation process *in situ*. *Ex situ* analytical TEM was conducted on a JEOL JEM 2100F, which is a 200KeV field-emission gun TEM/Scanning TEM (STEM) equipped with an analytical pole-piece, Oxford energy dispersive X-ray spectroscopy (EDS) system, and a Gatan Tridium system for electron-energy loss-spectroscopy (EELS) and elemental mapping, with 0.23 nm point resolution and 1 nm probe size for imaging and elemental analysis.

The XPS experiments were carried out in a UHV chamber equipped with an x-ray photoelectron spectrometer – SPECS Phoibos 100 MCD analyzer and an Ar^+ ion sputtering gun. The chamber typically has a base pressure of 2×10^{-10} Torr. A non-monochromatized Al-Kα X-ray source (hν= 1486.6 eV) was used for the XPS studies. The sample was heated via a ceramic button heater and its temperature monitored with a type-K thermocouple. The samples were annealed in the XPS chamber at 800℃in H_2 gas to remove the native oxide. Oxygen gas (purity = 99.9999%) was introduced to the system through a variable pressure leak valve and the sample was oxidized under a controlled pO_2 under the same conditions as *in situ* TEM experiments.

RESULTS AND DISCUSSION

Fig.1 (a) is the bright field TEM image of the Cu-5%Ni before H_2 exposure where the contrast could be due to strain from the native oxide. Fig. 1(b) is the corresponding select area electron diffraction (SAD) pattern revealing the (100)Cu-5%Ni formation where additional weak diffraction spots are due to the native oxide that formed during air exposure during the transport from the e-beam evaporator to the *in situ* UHV-TEM. After H_2 annealing *in situ*, the metal alloy film is smoother and the native oxide is removed (Fig. 1c and d).

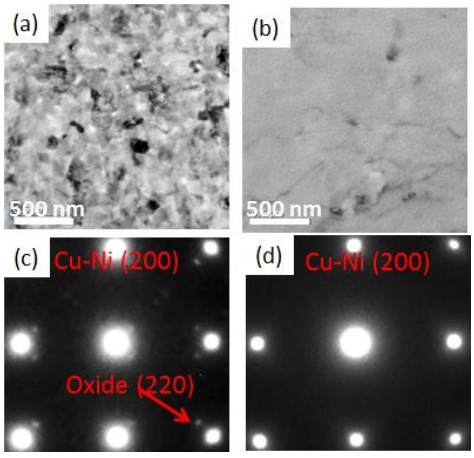

FIGURE 1. Comparison of the Cu-5at%Ni before and after 1 hour H_2 annealing at 750℃ and $pO_2=5\times10^{-4}$ Torr. (a) TEM bright field image showing the native oxide and strain contrast. (b) SAD pattern of (a) showing the existence of native oxide. (c) TEM bright field image showing the smooth and clean of the surface after annealing. (d) SAD pattern of (c) showing the removal of native oxide.

For the XPS experiments, the Ni 2p peak is used to identify the formation of NiO due to the clear changes of the XPS spectrum (see Fig. 2a).[31] Since Cu_2O and Cu have similar 2p XPS spectrum, we focused on the Cu LMM Auger peak to identify Cu_2O, which has a 2eV shift from metallic Cu (see Fig.

2b).[32, 33] The Cu-5%Ni films were also annealed in H_2 gas in the XPS chamber under the same conditions as the *in situ* UHV-TEM. The Fig.2 (a) and (b) show the clear shift of Ni 2p peak and Cu LMM peak obtain from the *in situ* XPS system after hydrogen annealing, which also demonstrates the reduction of the native oxide to its metallic state.

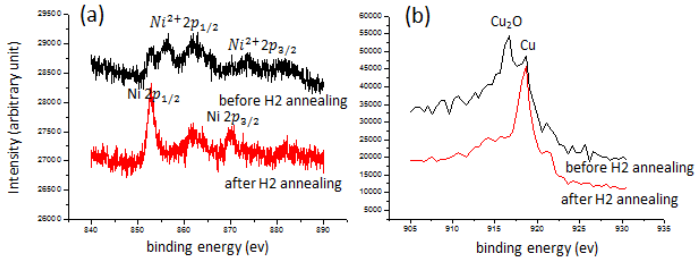

FIGURE 2. XPS data of the Cu-5at%Ni before and after H_2 annealing for 1 hour at 550 ℃ (a) The shift of Ni 2p peak after annealing indicating Ni oxides are reduced to Ni metal. (b) The shift of Cu LMM peak suggests reduction of the copper oxides to copper.

Figure 3 compares the Cu_2O island morphologies that formed during oxidation of pure Cu(100) to Cu-5at%Ni(100) at various temperatures. Since Cu_2O has simple cubic structure whereas NiO is fcc, the appearance of a (110) diffraction spots indicates Cu_2O formation. At 350℃, epitaxial Cu_2O oxide islands formed on the Cu-5at%Ni(100) surface similar to pure Cu, but the morphology of the islands are polyhedral not triangular in cross section in comparison to Cu(100). At 550℃, the appearance of the (220) diffraction spot without (110) diffraction spot indicates that NiO formed on the Cu-Ni surface not Cu_2O. The epitaxial relationship between oxide and the film changes from cube-on-cube to NiO (111)//CuNi (100) and NiO (220)//CuNi (220) at 700℃, the oxide is NiO but the islands are no longer epitaxial with respect to the Cu-Ni film as shown in the SAD ring pattern. We have previously reported a change of epitaxy of the Cu2O islands as function of oxidizing pressure.[34] Epitaxy is favored at low oxidizing pressures when the energy barrier to oxide nucleation is high and supply of oxygen is low, whereas high oxygen pressure enhances the rapid and the probability for random oxide nucleation. Similarly, the higher temperatures may favor NiO formation that may have a lower nucleation barrier than Cu_2O and thus favor random oxide nucleation.

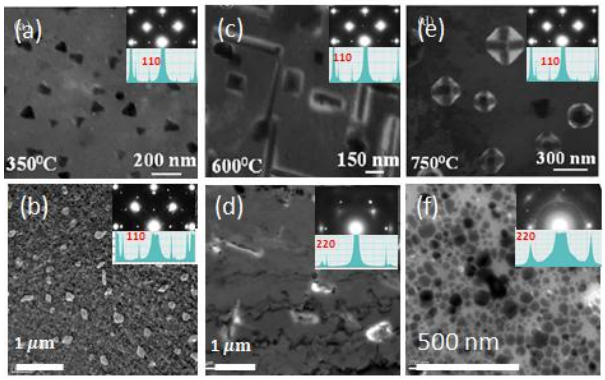

FIGURE 3. Comparison of the oxide islands formed on pure Cu and Cu-5at%Ni film under various temperatures and $pO_2=5\times10^{-4}$ Torr. The insets are the related SAD pattern. The existence of (110) indicates the formation of Cu_2O, otherwise, it is NiO formed on the surface. (a) Triangular Cu_2O oxide islands formed on the pure Cu surface at 350℃. (b) Polyhedral oxide islands formed on the Cu-5at%Ni surface at 350℃. (c) Rectangular and rod-like oxide islands formed on the pure Cu surface at 600℃. (d) Polyhedral and rod-like oxide islands formed on the Cu-5at%Ni surface at 550℃. (e) Cross-hatched oxide islands formed on the pure Cu surface at 750℃. (f) Dense and round oxide islands formed on the Cu-5at%Ni surface at 700℃.

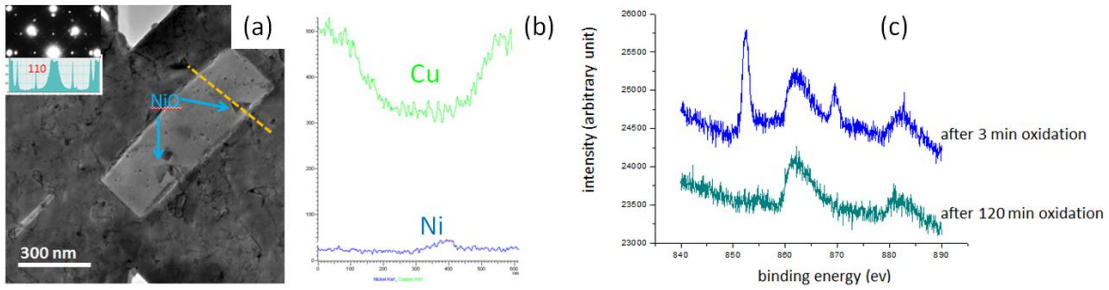

FIGURE 4. (a) TEM bright field image of small NiO islands on large Cu_2O island and related electron diffraction pattern. (b) Energy-dispersive X-ray spectroscopy (EDS) line-scan across the NiO and Cu_2O. (c) Ni 2p XPS data taken at 350℃ and $pO_2=5\times10^{-4}$ Torr as 3 and 120 minutes.

Since Cu_2O and NiO have similar lattice parameters, it is hard to distinguish NiO from Cu_2O using diffraction pattern. We used *ex situ* analytic TEM to detect nickel on the Cu_2O surface. Figure 4a is the bright field image of the Cu_2O oxide island where the small dark contrast contain Ni; the line indicates the position of the EDS line scan revealing Ni on the Cu_2O island (Fig. 4b). Figure 4c shows the Ni 2p XPS spectrum taken at 3 and 120 minutes oxygen exposure at $5x10^{-4}$ Torr O_2 and 350 ℃, where a significant NiO peak is noted after 120 minutes. XPS confirmed that NiO forms at 350 ℃ after oxidation long oxidation times indicating that these small islands on the Cu2O shown in Fig. 4a. Similar oxide duplex has been reported previously for Cu-Ni, but with Cu on the top of NiO.[35]

To further understand the sequential oxidation of NiO and Cu_2O, we examined the oxidation behavior of Cu-5at%Ni films at 550 °C by XPS and *in situ* UHV-TEM. Figure 6(a) shows the change of Ni 2p XPS spectrum during the oxidation at oxygen pressure of $5x10^{-4}$ Torr. Before oxidation, it shows clear metallic Ni 2p pattern. Only after a very short oxygen exposure time of 3 minutes, the Ni 2p peak indicates NiO. The Cu LMM peak shown in figure 3(b) did not change after 3 minutes of oxidation. After 30 minutes of oxidation, the Cu LMM peak reveals a small hump indicative of Cu_2O revealing the formation of a small amount of Cu_2O.

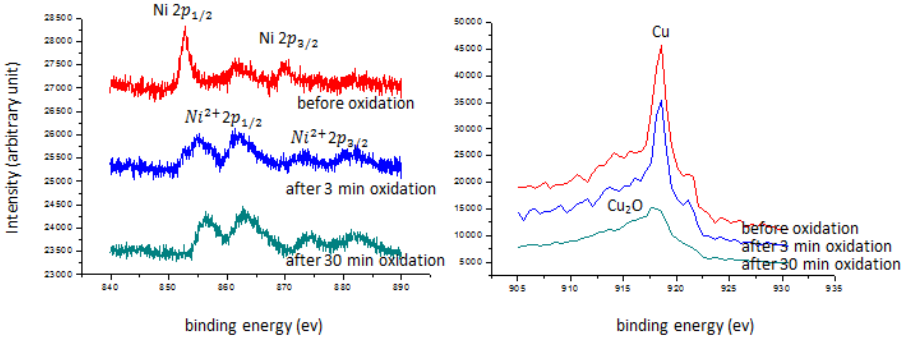

FIGURE 5. Oxidation in XPS system under 550℃ and $pO_2=5\times10^{-4}$ Torr. (a) The change of Ni 2p peak after oxidation. (b) The change of Cu LMM peak after oxidation.

The same experiment was performed in the *in situ* UHV TEM. Figure 6 is the bright field image of a NiO oxide island nucleation and growth. In comparison to Cu(100) oxidation under similar conditions,[28] the nucleation and growth of oxide islands on Cu-5at%Ni film are significantly faster. The nucleation density of oxide islands on the Cu-5at%Ni surface is 2 orders of magnitude lower than that on the pure Cu surface, the nucleation density of oxide islands on pure Cu surface is approximately $40/\mu m^2$ after 30 minutes oxidation, while the nucleation density of oxide islands on Cu-5at%Ni is only approximately $0.5/\mu m^2$ under the same condition. The oxide islands that formed on the Cu-5%Ni contain more defect and strain contrast in comparison to Cu; the oxide islands are polygon or irregular shape instead of rectangular shape found on pure Cu (see Fig 3c and 3d).

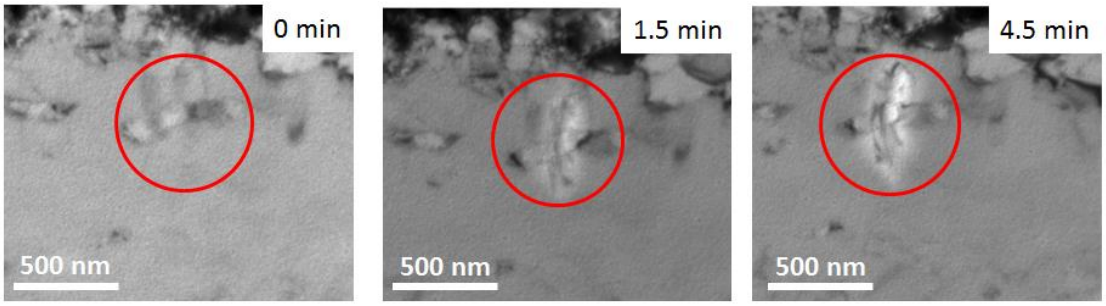

FIGURE 6. *In situ* observation of NiO island growth under 550℃ and $pO_2=1 \times 10^{-4}$ Torr. (a) Before oxidation. (b) After 1.5 minutes' oxidation. (c) After 4.5 minutes' oxidation.

Figure 7 compares the cross-sectional area growth of an NiO island on the Cu-5%Ni(100) to Cu_2O island on Cu(100). The growth of the Cu_2O island on Cu(100) is due to oxygen surface diffusion.[28] However, the growth rate of the oxide island on Cu-5%Ni(100) is parabolic, indicating a diffusion limited process for the oxide growth.

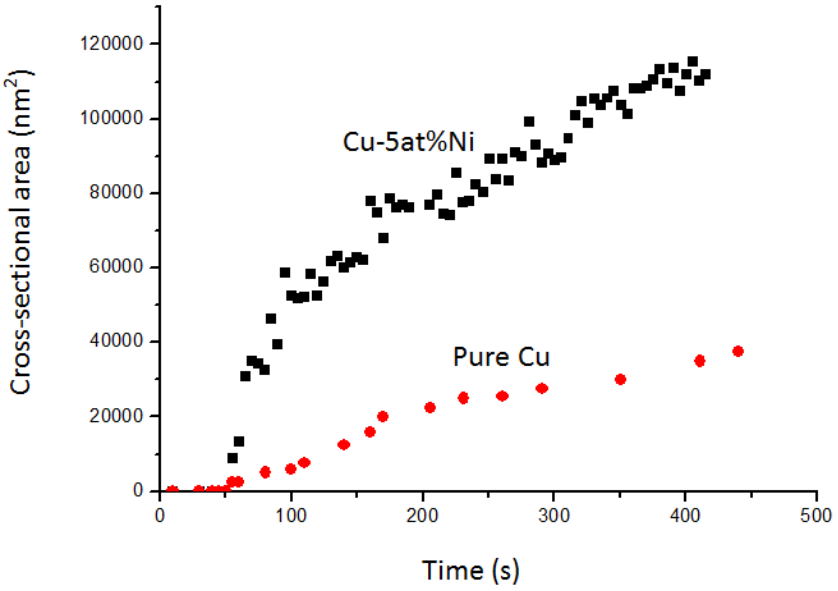

FIGURE 7. The temporal evolution of the size of the circled NiO island on Cu-5at%Ni, and comparison with the oxide island formed on pure Cu.

NiO is more thermodynamically stable than Cu_2O; it would be reasonable to expect NiO formation first. However, the *in situ* and *ex situ* TEM along with XPS experiments reveal a temperature dependant oxidation behavior for the initial oxide selection. We speculate that the temperature dependence of the Ni diffusion rate could explain the temperature dependent initial oxide selection. The diffusivities of Ni in Cu at various temperatures are displayed in table 1.[36] Table 1 shows that the diffusion length of Ni in Cu at 350 ℃ is only about 0.04 nm after 30 minutes, where Cu_2O islands form initially. Whereas at 550 ℃ where NiO islands form initially, the Ni diffusion length is comparable to the thickness of the Cu-Ni film. We suggest that at low temperatures, the Ni on the surface will oxidize quickly, but surface supply of Ni will deplete quickly and then Cu_2O will form rapidly. At higher temperature, the diffusion rate of Ni increases and its diffusion length becomes longer so that the supply of Ni to the alloy surface is plentiful and no longer limits the NiO growth.

TABLE 1. Comparison of the diffusivity of Ni in Cu under 350℃, 550℃ and 700℃.

	350℃	**550℃**	**700℃**
D (nm^2/s)	2×10^{-7}	2×10^{-2}	2
Time needed for the diffusion length reaches 40nm (minute)	3.3×10^{7}	3.3×10^{2}	3.3
Diffusion length for 30 minutes (nm)	0.04	12	120

CONCLUSION

The transient oxidation stage of Cu-5at%Ni(100) was investigated by complementary *in situ* and *ex situ* TEM and XPS tools to characterize the oxide identity and morphologies as function of oxidation time. Significant differences were noted between our earlier Cu(100) studies and the Cu-5%Ni alloys. A small increase of Ni content created a duplex NiO and Cu_2O islands. The selection of either NiO or Cu_2O to form initially depended on the oxidation temperature, which may be due to the temperature dependent diffusivity of Ni in Cu. Oxidation temperature also changed the epitaxy of the oxide islands from cube-on-cube to polycrystalline. The results here show the importance of temperature in controlling the microstructure of oxide during the oxidation of alloys. These observations of sequential and duplex oxide nucleation and growth should also apply to other alloys containing several oxidizing components.

ACKNOWLEDGMENTS

The authors thank M. France, L. Li and Z. Zhang for their assistance. This research program is supported by the National Science Foundation, Division of Materials Research (0706171). The *ex situ* TEM experiments were performed at NanoScale Fabrication and Characterization Facility, University of Pittsburgh. The XPS experiments were carried out at the Center for Functional Nanomaterials at Brookhaven National Laboratory, which is supported by the Department of Energy, Office of Basic Energy Sciences (DE-AC02-98CH10886).

REFERENCES

1. C. Wagner, Z. Phys. Chem. **21**, 25-41 (1933).
2. P. H. Holloway and J. B. Hudson, Surface Science **43**, 123-140 (1974).
3. T. M. Christensen, C. Raoul and J. M. Blakely, Applied Surface Science **26**, 408 (1986).
4. I. Vaquila, M. Passeggi and J. Ferron, J. Phys.: Condens. Matter **5**, A157-A158 (1993).
5. H. M. Kennett and A. E. Lee, Surface Science **48**, 633 (1975).
6. H. Brune, J. Wintterlin, R. J. Behm and G. Ertl, Phys. Rev. Lett. **68**, 624 (1992).
7. J. Jacobsen, B. Hammer, K. W. Jacobsen and J. K. Nørskov, Phys. Rev. B. **52**, 14954 (1995).
8. W. H. Orr, Cornell University, 1962.

9. K. Thurmer, E. Williams and J. Reutt-Robey, Science **297**, 2033-2035 (2002).
10. J. C. Yang, B. Kolasa, J. M. Gibson and M. Yeadon, Appl. Phys. Lett. **73**, 2841-2843 (1998).
11. J. C. Yang, M. Yeadon, B. Kolasa and J. M. Gibson, Scripta Materialia **38**, 1237-1241 (1998).
12. J. C. Yang and G. Zhou, Micron (0).
13. G. W. Zhou, W. S. Slaughter and J. C. Yang, Physical Review Letters **94**, 246101-246104 (2005).
14. G. W. Zhou and J. C. Yang, Surface Science **531**, 359-367 (2003).
15. G. Zhou and J. C. Yang, Journal of Materials Research **20** (7), 1684-1694 (2005).
16. J. C. Yang, L. Tropia and D. Evan, Appl Phys Lett **81**, 241-243 (2002).
17. J. C. Yang, M. Yeadon, B. Kolasa and J. M. Gibson, Appl Phys Lett **70** (26), 3522-3524 (1997).
18. J. C. Yang, M. Yeadon, B. Kolasa and J. M. Gibson, Scripta Materialia **38** (8), 1237-1242 (1998).
19. J. C. Yang, M. Yeadon, B. Kolasa and J. M. Gibson, Phil. Mag. **in preparation** (1998).
20. G. W. Zhou, L. Wang, R. C. Birtcher, P. M. Baldo, J. E. Pearson, J. C. Yang and J. A. Eastman, Physical Review Letters **96**, 226108-226110 (2006).
21. G. W. Zhou, L. Wang, R. C. Birtcher, P. M. Baldo, J. E. Pearson, J. C. Yang and J. A. Eastman, Journal of Applied Physics **101**, 033521-033526 (2007).
22. G. W. Zhou, X. Chen, D. Gallagher and J. C. Yang, Appl Phys Lett **93**, 123104-123106 (2008).
23. P. H. Holloway and J. B. Hudson, Surface Science **43** (1), 123-140 (1974).
24. P. H. Holloway and J. B. Hudson, Surface Science **43** (1), 141-149 (1974).
25. J. C. Yang and M. Yeadon, Appl Phys Lett **70** (26), 3522 (1997).
26. G. Y. Zhou, Judith C., Journal of Materials Research **20** (7), 1684-1694 (2005).
27. G. Zhou and J. C. Yang, Applied Surface Science **210** (3-4), 165-170 (2003).
28. G. Zhou and J. C. Yang, Physical Review Letters **89** (10), 106101 (2002).
29. G. Zhou, W. Slaughter and J. Yang, Physical Review Letters **94** (24), 246101 (2005).
30. M. L. McDonald, J. M. Gibson and F. C. Unterwald, Rev. Sci. Instrum. **60**, 700-707 (1989).
31. C. D. Wagner and G. E. Muilenberg, *Handbook of x-ray photoelectron spectroscopy: a reference book of standard data for use in x-ray photoelectron spectroscopy*. (Perkin-Elmer Corp., Physical Electronics Division, 1979).
32. S. Poulston, P. M. Parlett, P. Stone and M. Bowker, Surface and Interface Analysis **24** (12), 811-820 (1996).
33. L. Paul E, Journal of Electron Spectroscopy and Related Phenomena **4** (3), 213-218 (1974).
34. L. Luo, Y. Kang, Z. Liu, J. C. Yang and G. Zhou, Physical Review B **83** (15), 155418 (2011).
35. G. Zhou, D. D. Fong, L. Wang, P. H. Fuoss, P. M. Baldo, L. J. Thompson and J. A. Eastman, Physical Review B **80** (13), 134106 (2009).
36. T. Van Dijk and E. J. Mittemeijer, Thin Solid Films **41** (2), 173-178 (1977).